Search for Supersymmetry in a Three Lepton Plus Jets Signature

Pavel Zarzhitsky, Yuriy Ilchenko, Robert Kehoe, Peter Renkel, Ryszard Stroynowski

Southern Methodist University
Department of Physics
Dallas, Texas 75275-0175

Abstract

We present a method for searching for a three lepton plus jets supersymmetry signal at the ATLAS detector at $\sqrt{s} = 14$ TeV. The signal signature is three isolated leptons with p_T's above 5 GeV and two jets with p_T's above 40 GeV. We considered $t\bar{t}$, WZ, $Zb\bar{b}$ and Z+jets processes to be the main backgrounds. The signal extraction from the backgrounds was done using optimization cuts in five variables: p_T's of leptons, H_T and $\not{E}_T$. It was shown that the statistical significance exceeds $\rho = 5.4$ for 1 fb^{-1}. This allows a potential discovery of supersymmetry with 1 fb^{-1}.

CERN-THESIS-2008-200
01/11/2008

1 Introduction

The Standard Model (SM) is a very successful theory that explains all known experimental results. Nevertheless, it has some problems: the fine tuning needed for the Higgs mass (the hierarchy problem), the inability to account for observed weakly interacting matter dominating the universe ("dark matter"). If one wants to construct a more unified theory incorporating other interactions, then two other difficulties arise: there is a large gap in the particle spectrum between the electroweak energy scale and the Planck scale, and the extrapolation of running couplings do not converge simultaneously to one common value.

These problems inspire a search for physics beyond the SM. One of the most powerful SM extensions is called "supersymmetry" or SUSY. It is based on an assumption that there is one more spin symmetry in nature that relates fermions and bosons [1]-[3]. According to SUSY, each SM particle has a superpartner (sparticle) with the same properties, but different spin statistics. Supersymmetry provides a way to address some of these concerns:

- describe new physics that lies between weak and Planck energy scales.
- running couplings can be arranged to meet at the same point.
- the hierarchy problem is solved in a natural way.
- In many SUSY models, the lightest supersymmetric particle (LSP) is stable and if neutral it provides an excellent dark matter candidate.

1.1 Production and Decay of Supersymmetric Particles.

At hadron colliders sparticles can be produced through electroweak processes ([3]) including:

$$q\bar{q} \to \tilde{\chi}^+\tilde{\chi}^-,\ q\bar{q} \to \tilde{\chi}^0\tilde{\chi}^0, \tag{1}$$

$$q\bar{q} \to \tilde{\ell}^+\tilde{\ell}^-,\ q\bar{q} \to \tilde{\nu}_\ell\tilde{\nu}_\ell^*, \tag{2}$$

$$u\bar{d} \to \tilde{\chi}^+\tilde{\chi}^0,\ u\bar{d} \to \tilde{\ell}^+\tilde{\nu}_\ell, \tag{3}$$

$$d\bar{u} \to \tilde{\chi}^-\tilde{\chi}^-,\ q\bar{q} \to \tilde{\ell}^-\tilde{\nu}_\ell^*, \tag{4}$$

and QCD processes:

$$gg \rightarrow \tilde{g}\tilde{g},\ \tilde{q}\tilde{q}^*, \tag{5}$$

$$gq \rightarrow \tilde{g}\tilde{q}, \tag{6}$$

$$q\bar{q} \rightarrow \tilde{g}\tilde{g},\ \tilde{q}\tilde{q}^*, \tag{7}$$

$$q\bar{q} \rightarrow \tilde{q}\tilde{q} \tag{8}$$

QCD processes generally have much higher cross section unless they are forbidden by some conservation law. At the LHC the production through QCD should be dominating, unless squarks and gluinos are heavier then 1 TeV.

Our analysis is done for the coannihilation region where squarks have masses in the range 700-800 GeV, so QCD dominates. The coannihilation region is one of the regions in the SUSY parameter space consistent with the observed relic Weakly Interacting Massive Particle (WIMP) density [4]. The Lightest Supersymmetric Particle (LSP), in this case the lightest neutralino, has a mass of 130 GeV and perfectly fits to the cold dark matter requirements. The SUSY parameters (point SU1 [5]) chosen to represent the coannihilation region are $m_0 = 70$ GeV, $m_{\frac{1}{2}} = 350$ GeV, $A_0 = 0$, $\tan\beta = 10$, $sgn(\mu) = +$. The squark masses for the SU1 are all above 572 GeV, gluino mass is 832.33 GeV, LSP is lightest neutralino $\tilde{\chi}_1^0$, and its mass is 136.98 GeV, $\tilde{\chi}_2^0$ mass is 263.64 GeV, $\tilde{\chi}_1^+$ mass is 262.06 GeV, and $\tilde{e}$ mass is 154.06 GeV.

A trilepton signature is a valuable potential discovery mode for supersymmetry [6]. The signal event consists of three leptons, $\not{E}_T$ and hadronic jets. At LHC such signal can be obtained when one of the squarks or gluinos decays through $\tilde{\chi}_i^{\pm}$ and the other through χ_j^0, see Figure 1. The leptons from χ_j^0 must form a same flavor opposite sign pair. One of the three isolated leptons will have low p_T because of the SUSY coannihilation region particle spectrum.

This note is aimed at a search for a three lepton (e, μ) signature of SUSY event. The signal must contain a lepton pair of the same flavor and different charges plus a third lepton. Also, like any SUSY process, it must have large missing energy because the final state includes two LSPs. It also contains at least two high p_T jets. An example of such a decay chain is shown in Figure 1. This analysis was performed in the context of ATLAS trilepton analyses [6] which were omitting the coannihilation region due to the soft leptons. We have focused on the features of this region to explore the efficiency of a trilepton search there.

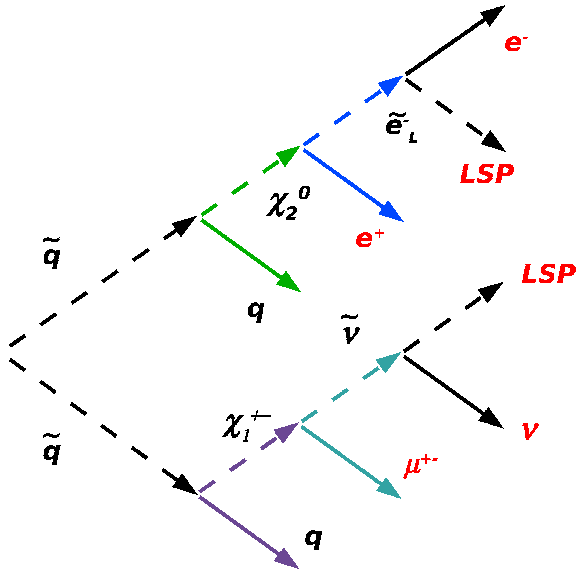

Figure 1: An example of the SUSY decay chain.

1.2 Possible Background Processes

There are several background processes that can produce three charged leptons. The first one is WZ when both bosons decay leptonically into three real, isolated leptons. This process results in low p_T jets and moderate $\not\!\!E_T$. Two other backgrounds are $t\bar{t}$ and $Zb\bar{b}$. They result in two isolated leptons from bosons decays plus the third, non isolated lepton from the semileptonic b decay. The main background process is $t\bar{t}$ production due to its medium $\not\!\!E_T$ and high p_T jets. The isolated leptons in the $t\bar{t}$ decay chain are coming from the leptonic W^+W^- decays, so they have the same charge but no flavor constraint. This allows us to use a same flavor, opposite sign requirement on the final state leptons to reduce the background. $Zb\bar{b}$ background results in a very small $\not\!\!E_T$ and high p_T jets. The last background process is $Z + jets$. This background can produce two real, isolated leptons from the leptonic Z decay and the third lepton as a fake from a jet. The jets can be energetic, but $\not\!\!E_T$ is low. The cross-sections [7] for the signal and backgrounds are given in Table 1.

Table 1: Leading order cross sections and event yields in 1 fb^{-1} for signal and backgrounds

process	cross section	branching ratio for 3ℓ	N_{events}
SUSY	7.3 pb	0.016	125.8
$t\bar{t}$	833 pb	0.021	17625
Zbb	1492 pb	0.046	68320
WZ	26 pb	0.035	910
$Z + jets$	5000 pb	0.06 * fake rate	99000

2 Triggering and Event Samples.

2.1 MC Samples

For the three lepton final state under study, there are three physics backgrounds (producing three real leptons) and an instrumental background (one of the leptons is a jet faking an isolated lepton). We have used simulation of these processes in release 12.0.6. The samples, their cross sections, the numbers of events, and sample IDs used in this study are summarized in Table 2.

Table 2: Monte Carlo samples and their cross sections as used in the analysis

signature	number of events	cross section, fb^{-1}	sample ID
SUSY	143000	7.3	5401
$t\bar{t} \to \ell + X$	382000	450	5200
$WZ \to \ell\ell\ell$	2500	0.3	6359
$Zbb \to \ell\ell\ell$	37150	15	5176
Z+jets, $Z \to ee$	43000	150	8132
Z+jets, $Z \to \mu\mu$	47000	150	8144

The properties of the Monte Carlo generation of each sample are:

- *SUSY "SU1" (coannihilation) point:* This is an inclusive sample, containing all possible decays, generated using HERWIG [8] with ISASUSY [9] providing the particle spectrum and branching ratios.
- *top-anti-top ($t\bar{t}$):* $t\bar{t}$ sample with at least one W produced in top decay decaying leptonically ($t\bar{t} \to \ell\nu X$). The sample was generated using HERWIG.

- *WZ:* includes only $WZ \to \ell\ell\ell\nu$, generated by HERWIG and using Jimmy [10] for underlying event simulation.

- *$Z + jets$: $Z \to e^+e^-$ or $Z \to \mu^+\mu^-$* together with two high p_T jets (jet p_T above 20 GeV). Generated by ALPGEN [11] plus HERWIG.

- *$Zb\bar{b}$:* $Zb\bar{b}$ $(Z \to \ell^+\ell^-,\ b \text{ or } \bar{b} \to \ell) \ \to \ell\ell\ell + X$, generated by PYTHIA [12].

2.2 Trigger Analysis

To estimate the response of the real detector we need to know what triggers are passed by the signal and what are the trigger efficiencies. Event $\not\!\!E_T$ is a standard feature of any SUSY decay chain due to two escaping LSP's. The only $\not\!\!E_T$ we could use in the trigger list appropriate to the reconstruction version we used (release 12.0.6) had 100% efficiency, but it was expected to be prescaled. For complete information about different trigger menus see [13]. Because of the relatively low p_T lepton that is expected at the coannihilation region, for the present analysis we considered the available triggers that are suitable for low p_T leptons.

- *EF_e10:* A single electron trigger at L1, L2 and EF. It starts with an electromagnetic cluster with $p_T > 5$ GeV at L1, and requires an electron with $p_T > 10$ GeV at L2 and EF. No isolation is required.

- *EF_e15iEF_e15i:* Two electron trigger. Starts with two electromagnetic clusters with $p_T > 15$ GeV. At L1 no isolation is applied. Two isolated electrons with $p_T > 15$ GeV are required at L2 and EF. The isolation cut is based on the calorimeter information only.

- *EF_mu6:* Single muon trigger. Starts with single muon with $p_T > 6$ GeV at L1, L2 and EF. No isolation is required.

Table 3: Trigger efficiencies.

Trigger item	eee	$ee\mu$	$\mu\mu e$	$\mu\mu\mu$
EF_ e10	1.000 ± 0.005	1.000 ± 0.003	1.000 ± 0.001	-
EF_ e15iEF_ e15i	0.792 ± 0.005	0.560 ± 0.003	-	-
EF_ mu6	-	0.821 ± 0.003	0.963 ± 0.001	0.98 ± 0.001

The final efficiencies at EF level are given in Table 3. They are almost 100%. We note that eventually each trigger used was decided to be prescaled. This would require use of triggers with higher p_T thresholds. Table 3 does indicate, however, a very high acceptance for the single lepton triggers. We assume in the results below that a logical OR of lepton and $\not\!\!E_T$ triggers available when data arrives will provide 100% trigger efficiency.

3 Lepton Identification and Isolation

Identification of leptons and their isolation from hadronic energy are critical to this analysis. We address these two issues separately below. In this discussion, we must calculate the efficiency for real electrons. This is calculated in general by matching reconstructed electrons to truth electrons from $W^{\pm}$, Z^0 or τ-decays in the SUSY sample. We define an efficiency to be the fraction of truth electrons that match within a cone of $\Delta R < 0.2$ to a reconstructed electron passing identification cuts. For efficiency, we consider two efficiencies: raw efficiency is the efficiency relative to the raw *eGamma* object level, and the isolation efficiency is calculated relative to the number of *eGamma* objects passing identification cuts.

We must also calculate a rate for jets to fake electrons. In almost all cases, we define the fake rate to be the fraction of *eGamma* objects in a dijet sample which pass the identification cuts. This fake rate is determined from a dijet sample, although other samples give roughly similar values. As with efficiency, we refer to two fake rates: raw fake rate is relative to raw *eGamma* object level, while the isolation fake rate is relative to the number of *eGamma* objects passing identification cuts. We also define an absolute fake rate as the probability for a jet, which at reconstruction level has no implicit EM energy fraction requirement such as in the *eGamma* algorithm, to fake an isolated lepton.

3.1 Lepton Identification

Electron identification cuts are summarized in a 12 bit $IsEM$ flag, [14], [15]. $IsEM$ = 0 is equivalent to tight; $IsEM$ & 3FF = 0 is equivalent to medium; $IsEM$ & 7 = 0 is equivalent to loose. We used selection cuts that are slightly looser then medium ($IsEM$ & 1f7=0, $IsEM < 3000$). We term these cuts "V1" to compare to medium electrons. The V1 identification does not use information from the first layer of the calorimeter and ignores some tracking information: the number of hits in

the pixel layer and SCT, and the track transverse impact parameter. To select these identification cuts, we compared the sensitivity of each $IsEM$ parameter at low and high p_T for both real and fake electrons, as defined above. The efficiencies and fake rates for the medium and V1 identification cuts are given in the first row of Tables 4 and 5, respectively. The V1 cuts are significantly more efficient than medium cuts with a similar fake rate.

Table 4: Comparison of efficiencies for standard medium electron identification cuts and suggested V1 identification cuts for electrons in the SUSY signal sample. The second row adds standard or V1 isolation cuts.

cuts	efficiency, medium	efficiency, V1
$IsEM$	0.76	0.89
+ isolation	0.73	0.75

3.2 Lepton Isolation

The signal has three isolated leptons while most of the backgrounds have at least one non-isolated one (consider the processes in Table 2 for a comparison of signal and backgrounds). For $t\bar{t}$ and $Zb\bar{b}$ backgrounds, the only way to get one of the leptons is to get it from the jet. It can be either a semileptonic b-quark decay, when a lepton is physically produced outside of the jet, but very close to it, or a jet fake, where the jet mimics an electron signal. The absolute jet fake rate is low (10^{-4}) [5], but leptons from b-quark decay are produced rather often (in approximately 17% of all b-quark decays for e and μ each).

The standard isolation variable is a transverse energy in a certain cone around the direction of the particle, minus the transverse energy of the particle itself. It is called "etcone" and is calculated for a set of different cone sizes. The standard isolation cut is $etcone(\Delta R < 0.2) < 10$ GeV. From the Table 5 you can see that standard isolation gives almost no rejection compare to the identification cuts. We found that $\frac{etcone(\Delta R)}{E_T(lepton)}$ is a more efficient cut. In the Figures 2 and 3 one can see isolation efficiencies for the different isolation cuts for the signal versus isolation fake rate of the $t\bar{t}$ background. The chosen cuts, $\frac{etcone(\Delta R<0.30)}{E_T(electron)} < 0.16$ and $\frac{etcone(\Delta R<0.20)}{E_T(muon)} < 0.14$, provide 0.86 relative efficiency for electrons, 0.91 relative efficiency for muons and 0.10 relative fake rate for each of them (V1 isolation cuts). From Tables 4 and 5 it is

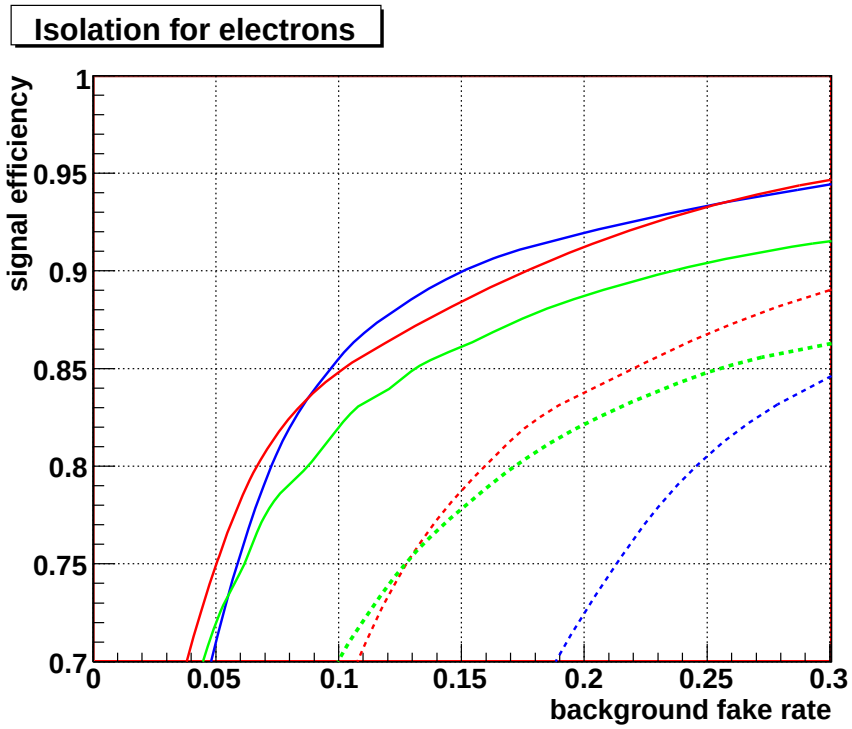

Figure 2: Isolation efficiency vs. fake rate for the identified electrons. The dashed curves are for the standard isolation variable, the solid curves are for the V1 isolations. Blue curves are for $\Delta R < 0.2$, red curves are for $\Delta R < 0.3$, green curves are for $\Delta R < 0.4$

clear that, after combining identification and isolation cuts, V1 cuts provide similar efficiency to medium cuts but give a large gain in fake electron rejection.

4 Optimization of Kinematic Selection

4.1 Event Preselection

The signal has three isolated leptons, large $\not\!\!E_T$ and more jet activity than background processes. These requirements define the cuts that we can use to separate signal from backgrounds. The lepton identification and isolation were already discussed above. The p_T's of the three leptons, $\not\!\!E_T$ and some jet variables are natural choices for the kinematic cuts. The p_T distribution of leptons for signal and backgrounds is shown in Figure 4. The lepton p_T's are similar for the signal and backgrounds. The p_T's of two leading jets are shown in Figure 5. Jets are reconstructed with a $\Delta R < 0.4$

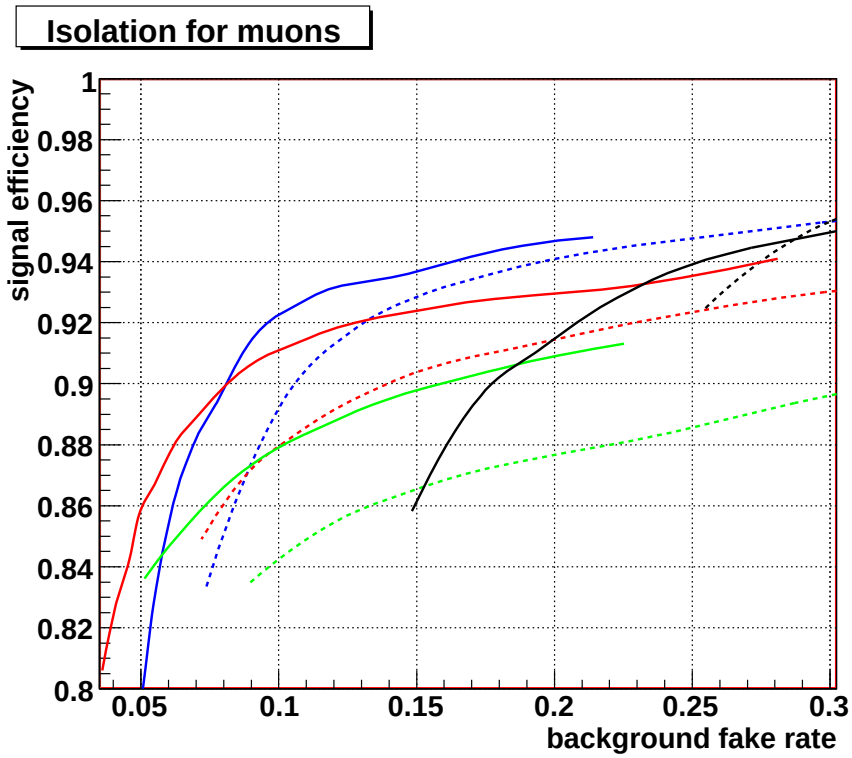

Figure 3: Isolation efficiency vs. fake rate for the identified muons. The dashed curves are for the standard isolation variable, the solid curves are for the V1 isolation. Black curves are for $\Delta R < 0.1$, blue curves are for $\Delta R < 0.2$, red curves are for $\Delta R < 0.3$, green curves are for $\Delta R < 0.4$

cone. Those within $\Delta R < 0.2$ of an isolated electron are omitted from the list of jets in each event.

First of all, let us define preselection cuts that have very high efficiency and define the signature of the signal. We choose the preselection cuts to be three isolated leptons above 5 GeV and two energetic jets above 40 GeV. The effect of the cuts on number of events is summarized in Table 6. The preselection cuts allow us to be sure that the main characteristics of the signal are in the selected events (except for $\not\!\!E_T$) and at the same time leave a lot of space for further selection during the optimization procedure.

Table 5: Comparison of fake rates for standard medium electron identification cuts and suggested V1 identification cuts for fake electrons from jets in a dijet sample. The second row adds isolation cuts.

Cuts	fake rate, medium	fake rate, V1
$IsEM$ cut	0.13	0.16
+ isolation	0.13	0.02

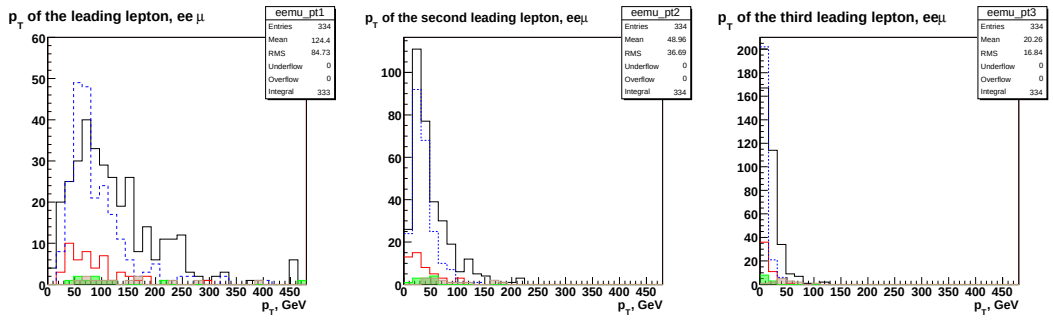

Figure 4: The p_T's of the leading lepton (left), the second leading lepton (middle) and the third leading lepton (right) for the signal and backgrounds. Black line is for SUSY, red one for $t\bar{t}$, dashed blue line is for $Zb\bar{b}$, green filled histogram is for WZ, brown filled histogram is for Zb+jets.

4.2 Optimization of Kinematic Selection

The current analysis is done for the early discovery possibility. That is why all the values of the cuts are selected to maximize the search sensitivity. To estimate the discovery potential a statistical significance parameter,

$$\rho = \frac{S}{\sqrt{S+B}}, \tag{9}$$

is used. Under the assumption that the search is limited by statistics, not systematic uncertainties, this figure should be reasonably correlated with the significance measured in the actual experiment. A significance of 5σ is considered sufficient for a discovery. The main goal of the signal selection optimization is to find a set of cuts that will maximize significance.

For the signal, the leptons come from χ_2^0 or $\chi_1^\pm$ decays. In the coannihilation region, one of the leptons from χ_2^0 is very soft, because the mass difference between initial

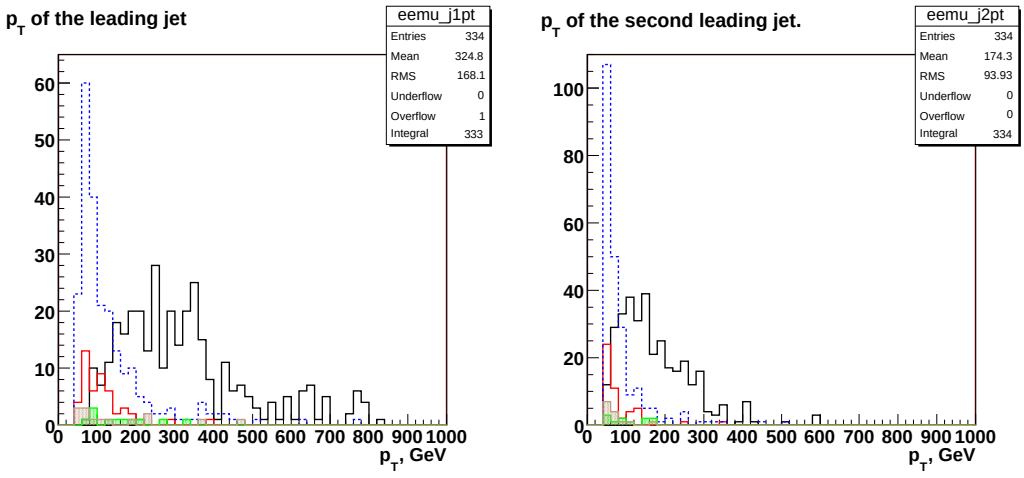

Figure 5: p_T's of the leading jet (left) and the second leading jet (right) for the signal and backgrounds. Black line is for SUSY, red one for $t\bar{t}$, dashed blue line is for $Zb\bar{b}$, green filled histogram is for WZ, brown filled histogram is for Zb+jets.

Table 6: Number of events in 1 fb^{-1} for the signal and backgrounds with different cuts applied

Process	3ℓ p_T >5 GeV	+isolation	+2 jets p_T >40 GeV
$SUSY$	800	80	72.9
$t\bar{t}$	23000	800	377
Zbb	16000	4200	1453.6
WZ	132	80	11.6
$Z+jets$	1056	152	159

and final particles is 10 GeV. Two leading leptons have the p_T's in the same range as the leading leptons from backgrounds, the comparison of p_T for all three leptons is shown in Figure 4. The lepton p_T's are similar for the signal and backgrounds.

$\not{E}_T$ is large for SUSY, because of two LSP's that escape the detector. It is also large for $t\bar{t}$ because of neutrinos from W decays. WZ, $Z+jets$ and $Zb\bar{b}$ have small $\not{E}_T$, that originates from jets by either their measurement and/or from very soft neutrinos from semileptonic heavy flavor quark decay. The $\not{E}_T$ is shown in Figure 6 on the left. The difference in jet activity should be taken into account. Instead of continuing to use the p_T's of the two leading jets as used for preselection, we decided to use a combined variable H_T

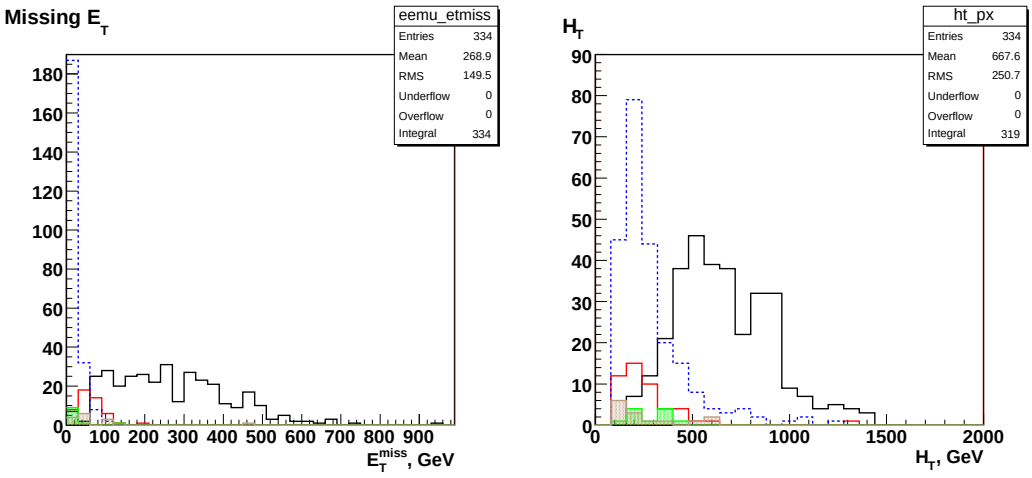

Figure 6: $\not\!\!E_T$ (left) and H_T (right) distributions for the signal and backgrounds. Black line is for SUSY, red one for $t\bar{t}$, dashed blue line is for $Zb\bar{b}$, green filled histogram is for WZ, brown filled histogram is for Zb+jets.

$$H_T = \sum_{alljets} E_T(jet). \tag{10}$$

We tried the sum of two leading jets only and the sum over all jets in the event. The latter choice is better because it takes into account the fact that SUSY events have more jets than WZ and $Zb\bar{b}$ events and a harder jet spectrum. The H_T distribution is shown in Figure 6 in the right plot. A minimal 5 GeV cut is low for electron and muon reconstruction and raises a question of whether the fake rate is under control. Its potential to impact the significance is discussed below. These reasons provide five optimization variables: $\not\!\!E_T$ and H_T, 3 lepton p_T's.

To check how the significance depends on these variables a grid search has been done. Extra cuts with varying thresholds were applied after preselection cuts. The $\not\!\!E_T$ threshold has a range from 0 to 460 GeV with step size 20 GeV. The H_T thresholds varied from 0 to 1000 GeV with step size 50 GeV. All three lepton p_T cut limits change from 5 to 14 GeV with the step size 1 GeV. For each point of the grid the significance was calculated. This allows to find the maximum and to check the dependence on different variables.

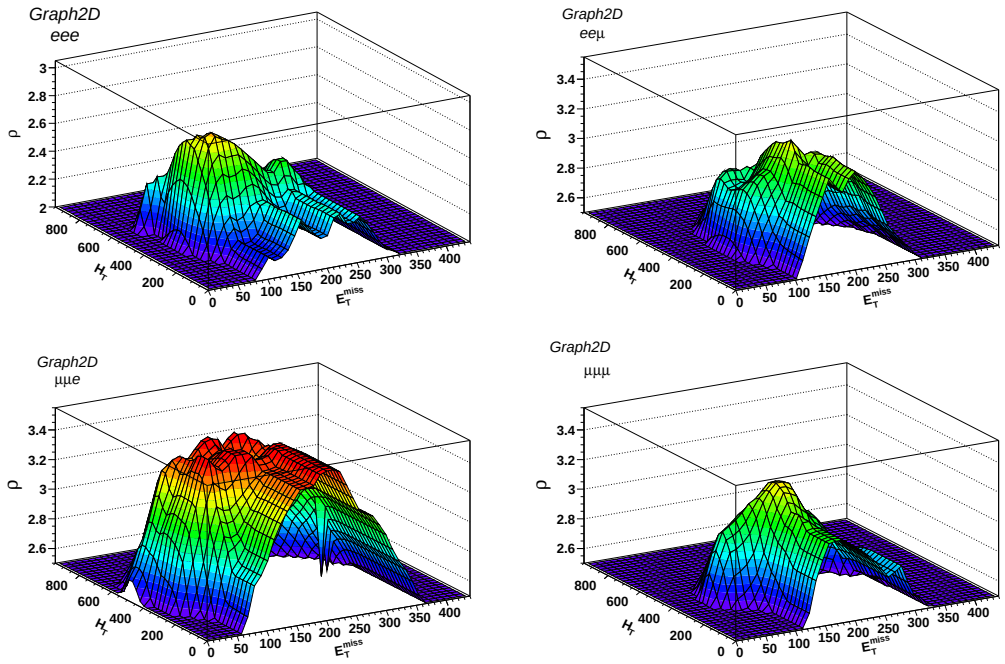

Figure 7: Optimization in $\not\!\!E_T$ and H_T, each channel separately, p_T of all leptons above 5 GeV. Step size is 50 for H_T and 20 for $\not\!\!E_T$. Top left plot is for eee, top right for $ee\mu$, bottom left for $\mu\mu e$ ans bottom right for $\mu\mu\mu$ channels.

4.3 Optimization in $\not\!\!E_T$ and H_T

We investigated each of the four channels by grid searching in the $\not\!\!E_T$ vs. H_T plane. Preselection cuts were applied. The significance dependence for each channel separately is shown at Figure 7. The x-axis gives the cut on H_T, the y-axis gives the cut on $\not\!\!E_T$, and the z-axis gives the significance ρ. The plot is smoothed between grid points. It is evident that all channels have a similar behavior, with $\rho = 3.0 - 3.6$. The positions of the maxima are given in Table 7.

4.4 Optimization in Lepton p_T

Now, let us check how significance depends on lepton p_T. $\not\!\!E_T$ and H_T cuts are set to be at the values from Table 7, events from all channels are grouped together. All cuts on lepton p_T's range from 5 to 14 GeV. We chose this range because tightening the p_T cut beyond 14 GeV to 30 GeV looses more signal than background. The S/B does not begin to improve until $p_T > 80$ or 100 GeV. By 150 GeV, the S/B is

Table 7: Cut values that provide maximum significance for each channel separately. All three leptons have $p_T > 5$ GeV, luminosity 1 fb^{-1}.

channel	$\not{E}_T$	H_T	$max(\rho)$
eee	> 100	> 350	3.0
$ee\mu$	> 160	> 250	3.3
$\mu\mu e$	> 140	> 300	3.6
$\mu\mu\mu$	> 160	> 350	3.3

better, but the significance is significantly lower because most signal events have been rejected. The result of our study are shown at Figure 8. The x- and y-axis are cuts on lepton p_T's, z-axis is significance ρ. The significance has almost no dependence on the leading lepton p_T in the given range, the dependence on the second lepton p_T is not very strong up to 8-9 GeV, but the lowest p_T lepton is rather sensitive. From this result, we conclude that the lepton p_T cuts should be 10, 7 and 5 GeV.

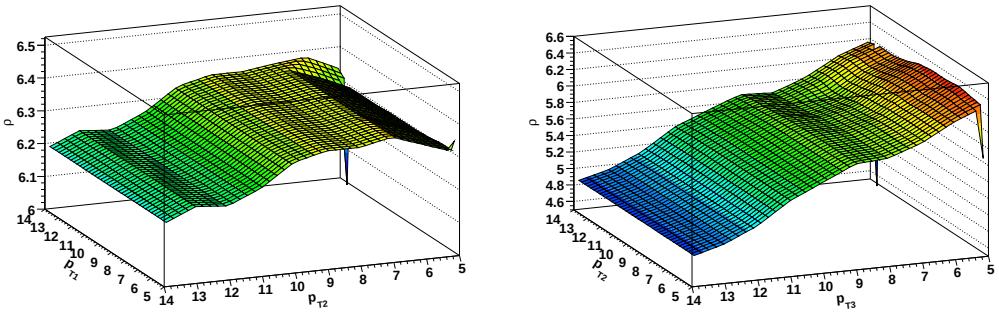

Figure 8: Optimization on lepton p_T using p_T's of two leading leptons (left) and p_T's of the second and third leading leptons (right).

4.5 Final Optimization.

The lepton p_T cuts are changed in the previous section, so we need to make a grid search in the $\not{E}_T$ vs. H_T plane again. Because of the similarity of the cuts in Table 7 the $\not{E}_T$ and H_T were changed simultaneously for all channels. The final optimization plot for all four channels is given in Figure 9. The events from all four channels were summed and then the significance was calculated for two sets of cuts given in Table 8. The maximum significance is 6.4, well above the discovery limit. If three leptons have

Table 8: Final cuts and significance in 1 fb^{-1}. A second point with 10 GeV cuts on all leptons is given for comparison.

p_{T1}	p_{T2}	p_{T3}	H_T	$\not{E}_T$	ρ
$>$ 10 GeV	$>$ 7 GeV	$>$ 5 GeV	$>$ 350 GeV	$>$ 140 GeV	6.4
$>$ 10 GeV	$>$ 10 GeV	$>$ 10 GeV	$>$ 350 GeV	$>$ 140 GeV	5.6

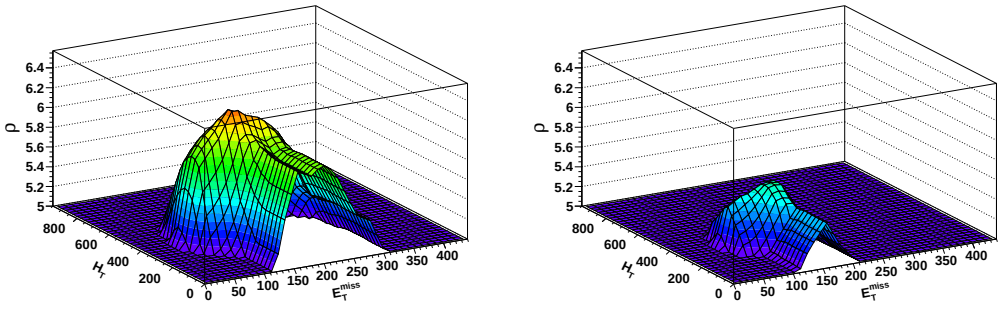

Figure 9: Optimization in $\not{E}_T$ and H_T, $p_{T1} > 10$ GeV, $p_{T2} > 7$ GeV, $p_{T3} > 5$ GeV (left) and optimization in $\not{E}_T$ and H_T, $p_{T1,2,3} > 10$ GeV (right).

$p_T > 10$ GeV, there is a drop in significance down to 5.6. The number of events for preselection and final cuts are shown in Table 9.

Table 9: Number of events after final cuts with statistical errors

process	N_{events} preselection cuts	N_{events} final cuts
$SUSY$	73 ± 9	57.1 ± 1.7
$t\bar{t}$	377 ± 19	17 ± 5
WZ	12 ± 3	0.15 ± 0.15
Zbb	$(1.45 \pm 0.04)10^3$	6 ± 3
$Z + jets$	189 ± 14	3 ± 3
$all\ BG's$	$(2.03 \pm 5)10^3$	26 ± 7
$significance$	1.6 ± 0.2	6.4 ± 0.6

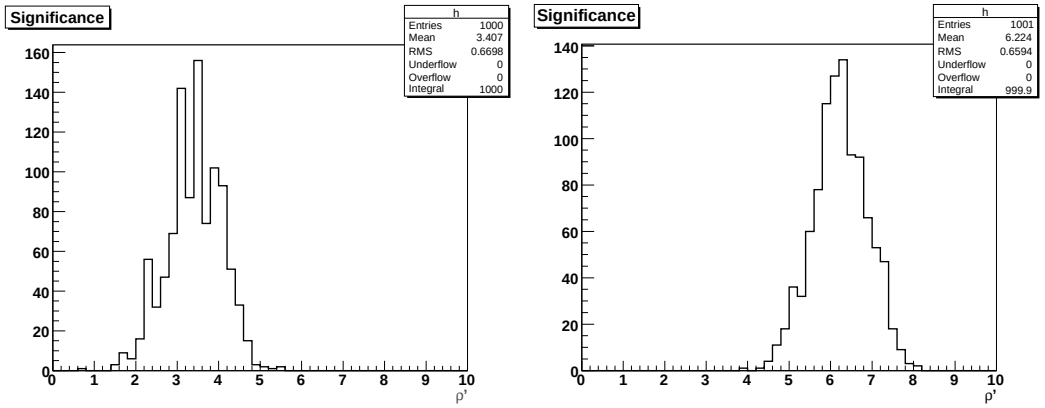

Figure 10: Sensitivity for 1 fb^{-1} (right) and 0.3 fb^{-1} (left).

5 Expected Sensitivity

5.1 Statistical Ensembles Testing

To properly account for statistical fluctuations, we need to make many pseudo-experiments ("ensembles"). The ensemble is an estimate of the number of events for the signal and backgrounds using random values that have Poisson distribution with mean equal to the number of events after final cuts (see Table 9). These data are used to calculate the significance ρ' for each ensemble. The significance was calculated as

$$\rho' = \frac{N_{SUSY} + N_{t\bar{t}} + N_{WZ} + N_{Zb\bar{b}} + N_{Z+jets} - \langle N_{BG} \rangle}{\sqrt{N_{SUSY} + N_{t\bar{t}+N_{WZ}+N_{Zb\bar{b}}+N_{Z+jets}}}}, \tag{11}$$

where $\langle N_{BG} \rangle$ is an average number of events for all background channels for each ensemble.

Table 10: Event yields and significance for several luminosity values. The $S/B = 2.04$.

luminosity, pb^{-1}	Number of signal events	Number of BG events	$\langle \rho' \rangle$
300	17	8.4	3.4
500	28	14	4.4
1000	57	28	6.2
2000	114	56	8.8

We performed the statistical analysis for 40 different luminosity points having 1000

ensembles at each point. The number of events were scaled from Table 9 to represent luminosity from 0 to 2 fb^{-1} with a step size 50 pb^{-1}. Two examples of the ρ' distribution are given in Figure 10. The significance at each luminosity point is a mean value calculated over 1000 ensembles. Fitting yields a statistical significance vs. luminosity of:

$$\rho' = (6.4 \pm 0.3)\sqrt{\text{luminosity}} - (0.03 \pm 0.03) \tag{12}$$

The values of the significance and the yields of signal and total background for several luminosity points are shown in Table 10. The discovery limit $\rho' = 5$ would be reached at 650 pb^{-1}.

5.2 Jet Calibration Uncertainty.

Table 11: Number of events for signal and backgrounds with and without shift in jet energy

process	N_{events} shift up	N_{events} without shift	N_{events} shift down
$SUSY$	58.3	57.1	55.3
$t\bar{t}$	21	17	17
WZ	0.44	0.15	0.15
Zbb	6	6	6
$Z + jets$	3	3	3
$all\ BG's$	30	26	26

These results depend largely on the quality of calibration, particularly of jets. The uncertainty in the jet energy scale early in the run will likely be large. This also impacts the $\not\!\!E_T$. So, this can cause substantial uncertainty in the significance. To account for this, we performed an artificial shift in the jet energy scale up and down by 10 % and checked the effect on the signal and background yield. The results are summarised in Table 11.

5.3 Jet Fake Rate Uncertainty.

The fake rate estimation using Monte Carlo data is not perfect and errors can be large [16]. That is why we decided to check how our final result depends on the fake rate. We calculated how the maximum significance depends on the fake rate,

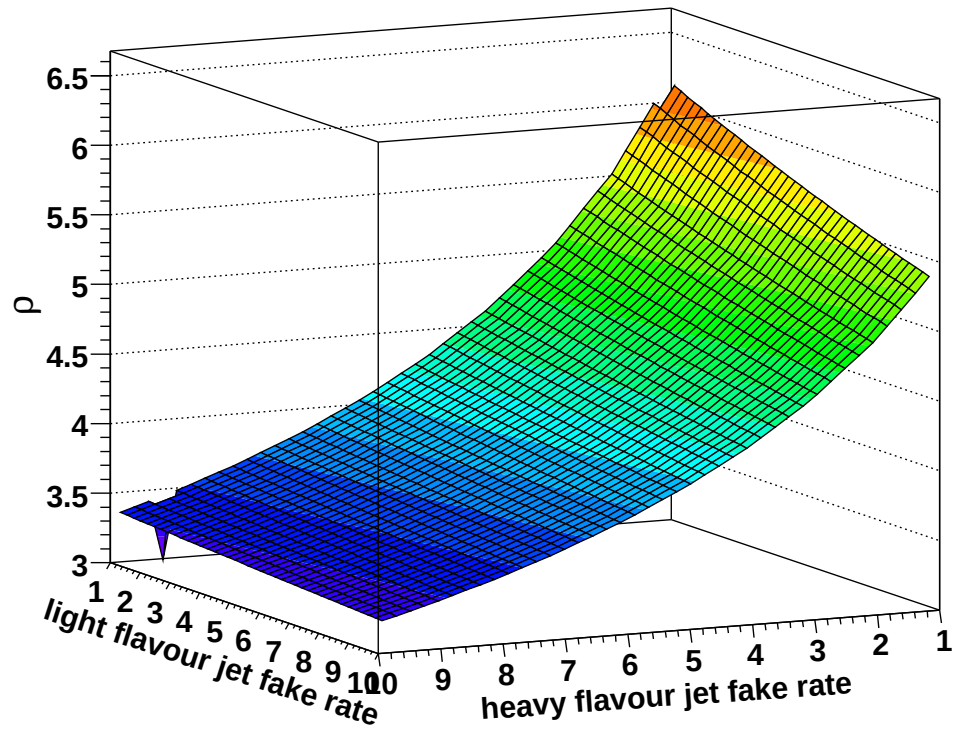

Figure 11: Maximum sensitivity depending on the relative heavy and light jet fake rates.

assuming that an increase of the fake rate by a certain factor provides the same increase in the number of background events.

There are two different kinds of fake leptons. The first one is when a light flavor jet mimics the lepton signal and passes the identification cuts. This type of fake is mostly present in $Z + jets$ background, where at least one of the final state leptons is a light flavor jet faking a lepton. The second type is when lepton is born in a b-quark semileptonic decay. In this case there is a real lepton present that has a part of the jet energy. Because of the large mass of the b-quark, this lepton can move aside from the main b-jet cluster and look like an isolated lepton. This type of fake provides one of the final state leptons for $t\bar{t}$ and $Zb\bar{b}$ backgrounds. The fake rates of both types are due to different physics reasons and uncorrelated with each other. Both fake rates were varied separately, the result of the study is shown at Figure 11. In the Figure 11, the maximum sensitivity depending on the multiplicative relative fake rates applied to the nominal heavy and light jet fake rates is shown. As you see, the final result is

much more sensitive to the relative heavy jet fake rate than to the light jet one. The discovery limit of $\rho = 5$ can be reached in 1 fb^{-1} if the heavy flavor jet fake rate is increased no more then twice, while the light flavor jet fake rate can be increased by an order of magnitude.

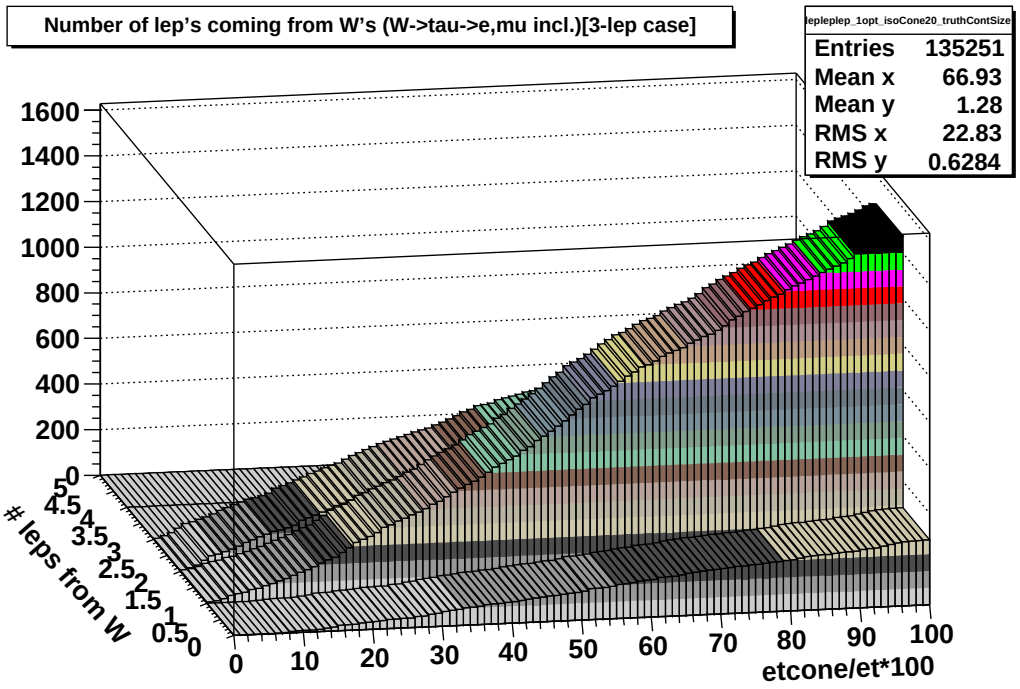

Figure 12: Estimate of event yield (z-axis) for the $t\bar{t}$ background vs. multiplicity of leptons from W boson decay and isolation cut.

We have studied the composition of the primary heavy flavor background, $t\bar{t}$, to address this issue. Approximately 41% of this background comes from the channel where one W boson decays leptonically and the other decays hadronically (i.e. lepton+jets channel). The remainder comes from the expected dilepton channel. As a result, varying the isolation cut (or the resulting fake rate) has a significant impact on this background and its composition, as can be seen in Figure 12.

To establish the magnitude of our uncertainty on eventual significance due to our lack of knowledge of the lepton fake rates, we have assumed an additional scenario beyond the nominal one. In this scenario the light flavor lepton fake rate is 100% higher than nominal while the heavy flavor fake rate is 50% higher. We have then estimated $\rho = S/\sqrt{S+B}$ as a function of isolation cut for the nominal and alternative scenarios. The results are shown in Figure 13 where the discrepancy increases with

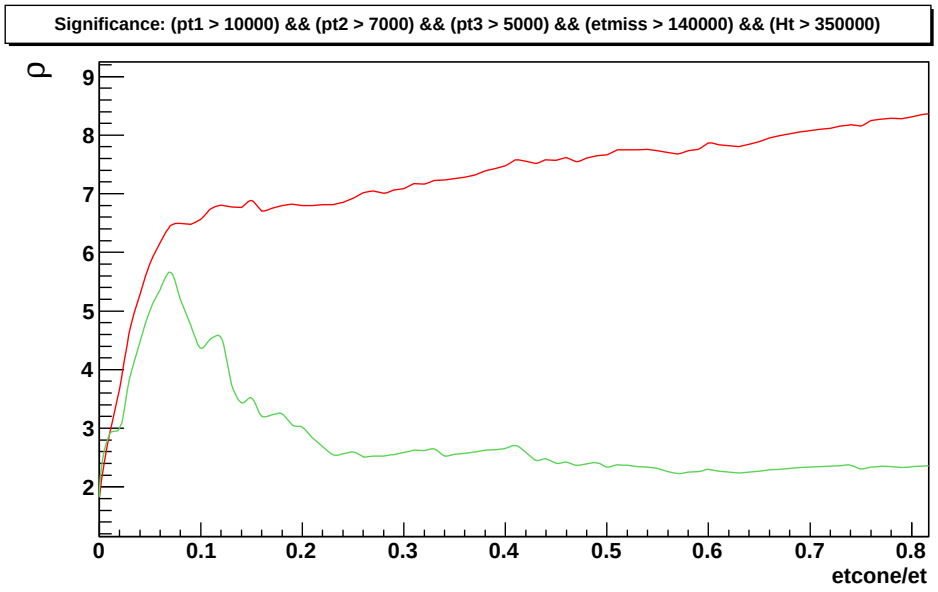

Figure 13: Estimate of significance vs. isolation cut for nominal and alternative fake rate scenarios.

looser isolation cut. In the case of worse than expected fake rates, a tighter isolation cut may be required. A cut of isolation < 0.07 would minimize this effect.

5.4 Inclusion of Systematic Uncertainties into Significance

We assume the systematic uncertainty on the event yield for the jet energy scale goes as described above. For the jet fake rate, the early data will provide a better estimate of fake rate than can be projected from the Monte Carlo. We expect the statistical uncertainty on the fake rate to be approximately 10% from QCD samples, and assume this level of uncertainty in the background event yields for all background processes. We assumed the jet energy scale and jet fake rate systematic uncertainties to be uncorrelated and found the systematic uncertainty on expected event yields by adding them in quadrature. The number of events and its statistical and systematic uncertainties for signal and backgrounds are shown at Table 12.

In order to include our systematic uncertainties from jet calibration and fake rate in our sensitivity, as well as statistical uncertainties on background event yield, we calculated a reduced significance [5]. This significance can be found from the probability for the background to fluctuate to the $S + B$, where B is distributed normally with

Table 12: Number of events after final cuts with statistical and systematic errors. The systematic uncertainty is the sum in quadrature of jet energy scale and fake rate uncertainties.

process	N_{events} final cuts	σ_{stat}	σ_{syst}
$SUSY$	57.1	1.7	+1.3/-1.7
$t\bar{t}$	17.	5	+3.9/-1.7
WZ	0.15	0.15	+0.33/-0.15
Zbb	6	3	+0.6/-0.6
$Z + jets$	3	3	+0.3/-0.3
$allBG's$	26	6	+4.0/-1.9

the total measured uncertainty. The probability is given by:

$$p = \int_0^\infty G(b; B, dB) \sum_{i=S+B}^{\infty} P(i; b), \tag{13}$$

where $G(b; B, dB)$ is a normal distribution with mean of B and width of dB, and $P(i)$ is a Poisson distribution with mean of b. The significance is then given by:

$$Z_n = \sqrt{2}\,\mathrm{erf}^{-1}(1 - 2p) \tag{14}$$

The reduced significance is found to be 5.4 in 1 fb^{-1}. This reduction comes mainly from the limited statistics in our current background Monte Carlo samples, most notably the ($t\bar{t}$) sample. It does not come from actual systematic effects. Only a handful of events pass our selection cuts in these samples. If ATLAS had an order of magnitude larger statistics (either from data or Monte Carlo) for background estimation, our significance would be 6.3 in 1 fb^{-1}.

6 Results

The presented analysis indicates the possibility of an early SUSY discovery in the coannihilation region. We have studied physics backgrounds and should be able to identify the signal. We estimate the significance to be 5.4σ in 1 fb^{-1}. However, this is just an estimate from below on the actual value of the significance and limited by the current statistics in background estimation. Reducing the statistical uncertainty on the expected background event yield by a factor of 10 raises the significance to 6.3σ.

7 Acknowledgement

We wish to thank Antonella de Santo for her helpful feedback during the work on this analysis. Azeddine Kasmi was also helpful in matters of electron identification.

References

[1] S. Dimopoulos and H. Georgi, "Softly Broken Supersymmetry And SU(5)," Nucl. Phys. B **193**, 150 (1981).

[2] S. Dimopoulos, S. Raby and F. Wilczek, "Supersymmetry And The Scale Of Unification," Phys. Rev. D **24**, 1681 (1981).

[3] S.P. Martin. *A Supersymmetry Primer. hep-ph/97-9356, June 2006.*

[4] M. Battaglia, I. Hinchliffe and D. Tovey, J. Phys. G **30**, R217 (2004) [arXiv:hep-ph/0406147].

[5] Expected Performance of the Atlas Experiment Detector, Trigger and Physics, G. Aad et al., arXiv:0901.0512 (2009)

[6] C. Potter, A. De Santo, J. Dragic, "Trilepton SUSY Signatures at ATLAS", ATL-COM-PHYS-2008-060 (2008).

[7] SUSY working group wiki page, https://twiki.cern.ch/twiki/bin/view/Atlas/SUSYWorkingGrou

[8] G. Corcella "HERWIG 6.5 Release Note" hep-ph/0210213 (2002).

[9] F. Paige, S. Protopopescu, H. Baer, X. Tata, ISAJET 7.69 A Monte-Carlo Event Generator, hep-ph/0312045 (2003).

[10] J. Butterworth, J. Forshow, M. Seymour, Multiplication interactions in photo-production at HERA, Z. Phys. C72:637-646 (1996).

[11] M. Mangano, et al., J. High Energy Phys. 07, 001 (2003).

[12] T. Sjostrand, S. Mrenna, P. Skands, PYTHIA Physics and Manual, hep-ph/0603175 (2006).

[13] *ATLAS Trigger Working Group web page*
https://twiki.cern.ch/twiki/bin/view/Atlas/TapmMainPage

[14] ATLAS Collaboration. *Expected Performance of the ATLAS Experiment, Detector, Trigger and Physics.*. CERN-OPEN-2008-020, Geneva, 2008.

[15] ATLAS Collaboration. *The ATLAS Experiment at the CERN Large Hadron Collider*. JINST 3 (2008) S08003.

[16] O. Brandt, A. Barr, P. de Renstrom, ATL-PHYS-INT-2008-023 (2008).